RANGE SHIFTS

Unexpected westward range shifts in European forest plants link to nitrogen deposition

Pieter Sanczuk[1]*, Kris Verheyen [1], Jonathan Lenoir[2], Florian Zellweger[3], Jonas J. Lembrechts[4,5], Francisco Rodríguez-Sánchez[6], Lander Baeten[1], Markus Bernhardt-Römermann[7,8], Karen De Pauw[1], Pieter Vangansbeke[1], Michael P. Perring[9,10], Imre Berki[11], Anne D. Bjorkman[12,13], Jörg Brunet[14], Markéta Chudomelová[15], Emiel De Lombaerde[1]†, Guillaume Decocq[2], Thomas Dirnböck[16], Tomasz Durak[17], Caroline Greiser[18,19], Radim Hédl[15,20], Thilo Heinken[21], Ute Jandt[8,22], Bogdan Jaroszewicz[23], Martin Kopecký[24,25], Dries Landuyt[1], Martin Macek[24], František Máliš[26,27], Tobias Naaf[28], Thomas A. Nagel[29], Petr Petřík[15,30], Kamila Reczyńska[31], Wolfgang Schmidt[32], Tibor Standovár[33], Ingmar R. Staude[8,34], Krzysztof Świerkosz[35], Balázs Teleki[36], Thomas Vanneste[1], Ondrej Vild[15], Donald Waller[37], Pieter De Frenne[1]

Climate change is commonly assumed to induce species' range shifts toward the poles. Yet, other environmental changes may affect the geographical distribution of species in unexpected ways. Here, we quantify multidecadal shifts in the distribution of European forest plants and link these shifts to key drivers of forest biodiversity change: climate change, atmospheric deposition (nitrogen and sulfur), and forest canopy dynamics. Surprisingly, westward distribution shifts were 2.6 times more likely than northward ones. Not climate change, but nitrogen-mediated colonization events, possibly facilitated by the recovery from past acidifying deposition, best explain westward movements. Biodiversity redistribution patterns appear complex and are more likely driven by the interplay among several environmental changes than due to the exclusive effects of climate change alone.

One of the most prominent biogeographical changes of the 21st century is the large-scale redistribution of plants and animals in response to changes in the climate system (*1*). Warming temperatures are causing many terrestrial species to move toward higher latitudes and elevations, which results in a reordering of species' distributions (*1*–*3*) and the emergence of novel communities (*4*). Empirical evidence has been reported for a wide range of ecosystems and taxa—from poleward and upslope range shifts in temperate regions (*5*, *6*) and high-latitude boreal biomes (*7*) to upslope shifts in mountain vegetation (*8*)—which suggests an emerging link with anthropogenic climate warming (*2*, *9*).

According to the most recent global synthesis (*1*), terrestrial species are shifting toward higher latitudes at an average rate of 1.11 km year^{-1}. This trend, however, lacks statistical significance, possibly because estimates are often blurred by variation in methodological attributes (*1*, *10*). Alternatively, species' redistributions in geographical directions that are orthogonal (i.e., west–east oriented) or even inverse (e.g., equatorward) to the moving isotherms are less likely to be detected from commonly studied range boundary shifts along thermal transects of latitude and elevation alone (*11*, *12*). Indeed, other prominent environmental changes such as atmospheric (nitrogen and sulfur) deposition and forest disturbances show spatial patterns that are weakly correlated to the geographic direction of climate change (*13*–*15*) and can also influence demographic processes of colonization and local extinction (*1*, *12*, *16*). To what ex… these other environmental changes are … tributing to species range shifts remains largely unquantified (*17*–*19*).

Here, we quantify the rate and geographic direction of range shifts in 266 European forest understory plant species using multidecadal community data collected in mature forest stands across 2954 resurveyed semipermanent vegetation plots (*20*) (Fig. 1A). Plant community data were derived from baseline surveys recorded between 1933 and 1994 and paired resurveys carried out after the baseline surveys between 1987 and 2017 [median (minimum to maximum) intersurvey interval: 39 (13 to 67) years]. We quantified the shifts of species' distributions within the spatial extent of the study area on the basis of range centroids, i.e., the abundance-weighted geometric center of a species' distribution (fig. S1). In contrast to the more frequent quantification of range boundary shifts at the trailing or leading edges, analyzing centroid shifts allows us to obtain more robust estimates of the magnitude and geographic direction of complex distribution shifts (*6*, *11*, *21*). This is important because range shift estimates from leading and trailing edges alone are more prone to bias from stochastic processes or low sample sizes that may blur overall biogeographical trends (*11*).

The rate and geographic direction of centroid shifts

To calculate the centroid shift of each species, we first located the position of the abundance-weighted centroid at the time of the baseline survey and the resurvey and assessed the magnitude (i.e., the distance) and geographical direction (i.e., the bearing) of the centroid shift over time. Centroid shifts were expressed as the absolute shift rate (km year^{-1}) as well as the projected south–north (km north year^{-1}) and west–east (km east year^{-1}) rate (schematically explained in fig. S1). Centroid shifts were calculated for the 266 species that were

Downloaded from https://www.science.org at Universitaetsbibliothek Bern on October 15, 2024

[1]Forest & Nature Lab, Department of Environment, Ghent University, Melle-Gontrode, Belgium. [2]UMR CNRS 7058 "Ecologie et dynamique des systèmes anthropisés" (EDYSAN), Université de Picardie Jules Verne, Amiens, France. [3]Forest Resources and Management, Swiss Federal Research Institute WSL, Birmensdorf, Switzerland. [4]Research Center on Plants and Ecosystems (PLECO), University of Antwerp, Wilrijk, Belgium. [5]Ecology & Biodiversity (E&B), Utrecht University, Utrecht, the Netherlands. [6]Departamento de Biología Vegetal y Ecología, Universidad de Sevilla, Sevilla, Spain. [7]Institute of Ecology and Evolution, Friedrich Schiller University Jena, Jena, Germany. [8]German Centre for Integrative Biodiversity Research (iDiv) Halle-Jena-Leipzig, Leipzig, Germany. [9]Environment Centre Wales, UKCEH (UK Centre for Ecology and Hydrology), Bangor, UK. [10]The UWA Institute of Agriculture, The University of Western Australia, Perth, Australia. [11]Faculty of Forestry, Institute of Environmental and Earth Sciences, University of Sopron, Sopron, Hungary. [12]Department of Biological and Environmental Sciences, University of Gothenburg, Gothenburg, Sweden. [13]Gothenburg Global Biodiversity Centre, Gothenburg, Sweden. [14]Southern Swedish Forest Research Centre, Swedish University of Agricultural Sciences, Lomma, Sweden. [15]Department of Vegetation Ecology, Institute of Botany, Czech Academy of Sciences, Brno, Czech Republic. [16]Ecosystem Research and Environmental Information Management, Environment Agency Austria, Vienna, Austria. [17]Institute of Biology, University of Rzeszów, Rzeszów, Poland. [18]Department of Physical Geography, Stockholm University, Stockholm, Sweden. [19]Department of Forest Ecology and Management, Swedish University of Agricultural Sciences, Umeå, Sweden. [20]Department of Botany, Palacký University in Olomouc, Olomouc, Czech Republic. [21]Institute of Biochemistry and Biology, University of Potsdam, Potsdam, Germany. [22]Institute of Biology/Geobotany and Botanical Garden, Martin-Luther-University Halle-Wittenberg, Halle/Saale, Germany. [23]Faculty of Biology, Bialowieza Geobotanical Station, University of Warsaw, Bialowieza, Poland. [24]Department of Geoecology, Institute of Botany of the Czech Academy of Sciences, Průhonice, Czech Republic. [25]Faculty of Forestry and Wood Sciences, Czech University of Life Sciences Prague, Prague, Czech Republic. [26]Department of Phytology, Technical University in Zvolen, Zvolen, Slovakia. [27]National Forest Centre, Zvolen, Slovakia. [28]Leibniz Centre for Agricultural Landscape Research (ZALF), Muencheberg, Germany. [29]Department of Forestry and Renewable Forest Resources, Biotechnical Faculty, University of Ljubljana, Ljubljana, Slovenia. [30]Department of Ecology, Faculty of Environmental Sciences, Czech University of Life Sciences Prague, Czech Republic. [31]Independent researcher, Wrocław, Poland. [32]Department of Silviculture and Forest Ecology of the Temperate Zones, University of Goettingen, Göttingen, Germany. [33]Department of Plant Systematics, Ecology and Theoretical Biology, Institute of Biology, ELTE Eötvös Loránd University, Budapest, Hungary. [34]Institute of Biology, Leipzig University, Leipzig, Germany. [35]Museum of Natural History, University of Wrocław, Wrocław, Poland. [36]HUN-REN–UD Biodiversity and Ecosystem Services Research Group, University of Debrecen, Debrecen, Hungary. [37]Botany, University of Wisconsin–Madison, Madison, USA.

***Corresponding author. Email: pieter.sanczuk@ugent.be**

†Present address: Research Institute for Nature and Forest, Brussels, Belgium.

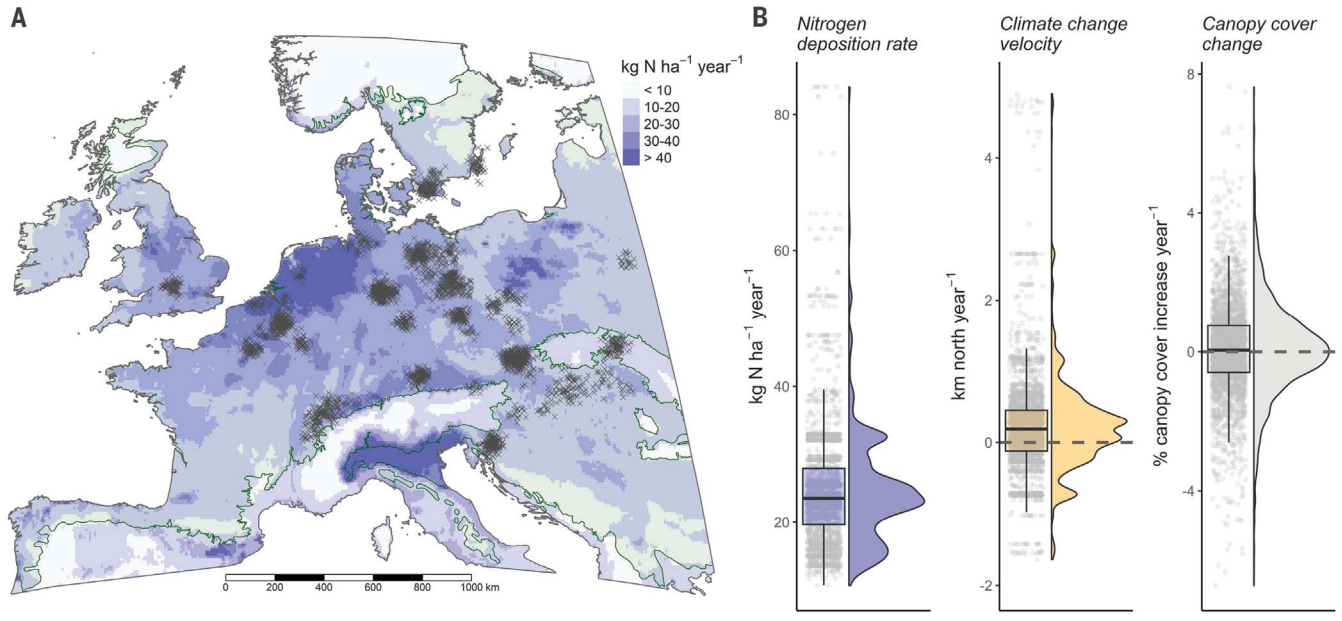

Fig. 1. Spatial and environmental gradients of the study. (**A**) Map of modeled nitrogen (N) deposition rate (sum of oxidized and reduced wet and dry deposition expressed in kg N ha^{-1} year^{-1}; dry deposition accounted for deciduous forest surface) at 0.1° resolution for the reference year 2000 and distribution of the 2954 resurveyed vegetation plots (gray crosses, spatially jittered for clarity) across the European temperate forest biome (shaded green background) (*20*). (**B**) Observed environmental variation across the 2954 vegetation plots (gray dots) of three key drivers of forest biodiversity over the course of the study period investigated here: nitrogen deposition rate (total of oxidized and reduced wet and dry N), climate-change velocity (realized changes of both temperature and precipitation, expressed in km north year^{-1}), and the rate of canopy cover change (average annual rate; expressed in % canopy cover increase year^{-1}). In all boxplots, we present the median (horizontal line), first and third quantile (lower and upper hinges), and 1.5 times the interquartile range (whiskers). Half violin plots represent the density distributions of the environmental change values. The gray dashed lines represent no changes (not shown for nitrogen deposition rates). Negative values in the case of climate and canopy cover change indicate southward velocities and canopy opening, respectively.

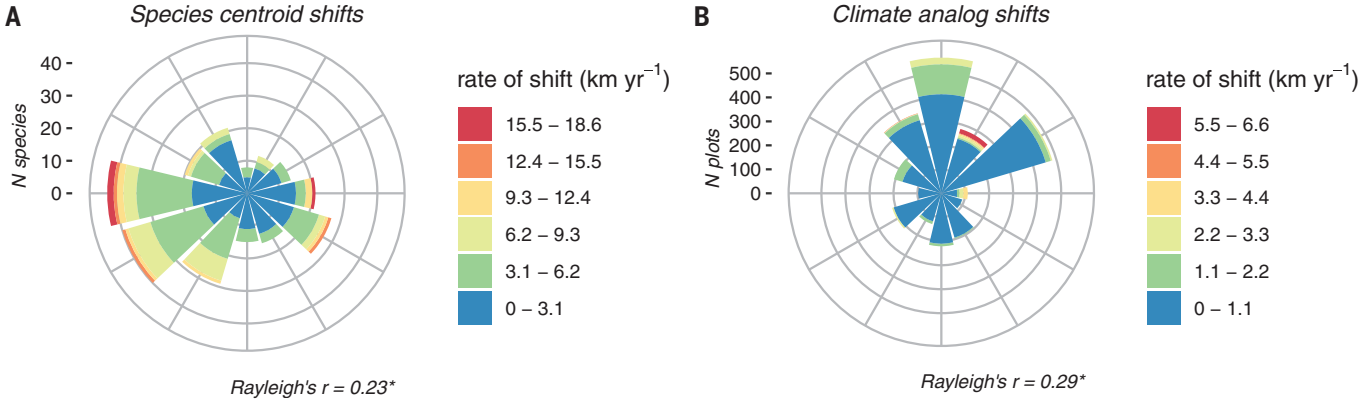

Fig. 2. Rate and geographic direction of species centroid shifts and climate analog shifts. (**A**) Rate and geographic direction of species range centroid shifts (*n* species = 266). (**B**) Velocity and geographic direction of climate analog shifts (*n* plots = 2,954). In all graphs, the Rayleigh's *r* statistic represents a test of uniformity that compares the bearings of shifts to a uniform circular distribution (null hypothesis). Larger values indicate more directional shifts. Asterisk (*) indicates significant deviations from the null hypothesis ($P < 0.05$). See figs. S3 and S4 for results of the analyses including rare species and per biogeographic region.

recorded in ≥1% of the plots to increase robustness of the estimates. The directionality (i.e., angular dispersion of the directions of centroids shifts) across all species was tested by using the Rayleigh's *r* coefficient, a circular regression coefficient that quantifies how uniform and isotropic the directions of shifts are (Rayleigh's $r = 1$ if all species are moving in the same direction, whereas Rayleigh's $r = 0$ with random directional movements, i.e., anisotropic, meaning that directions of shifts can be drawn from a uniform circular distribution).

Species' centroid shifts were first compared to the velocity and direction of climate change realized over the course of the study period. Spatially explicit climate-change velocities were calculated by climate analog mapping (*22*, *23*), an approach that is theoretically equivalent to the mapping of species centroid shifts (fig. S1). In contrast to the frequent calculation of climate-change velocities on the basis of gradients of isotherms alone (*3*, *24*), climate analog mapping allows us to consider consolidated changes of multiple bioclimatic variables at

Downloaded from https://www.science.org at Universitaetsbibliothek Bern on October 15, 2024

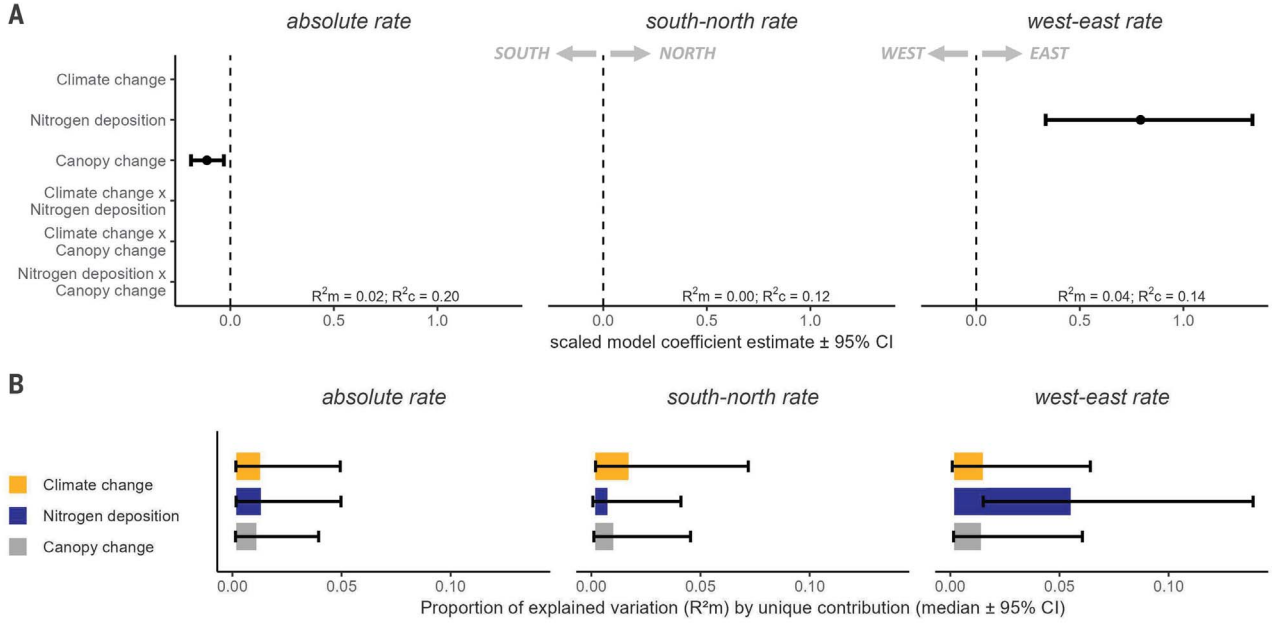

Fig. 3. Effects of environmental changes on centroid shifts based on the most parsimonious model. (**A**) Results of the mixed-effects models (*n* species = 266) indicating coefficient estimates and 95% confidence intervals (CIs) of the effects of the velocity of climate change (km year^{-1}, km north year^{-1}, km east year^{-1}), average nitrogen deposition rate between the baseline survey and resurvey (kg N ha^{-1} year^{-1}), and rate of canopy change (% cover increase year^{-1}), as well as all pairwise interactions (indicated with "×") on the absolute rate of centroid shifts (km year^{-1}) and the south–north rate (km north year^{-1}; negative values indicate southward shifts) and west–east rate (km east year^{-1}; negative values indicate westward shifts) extracted from the most parsimonious model structure (empty rows were not included in the final selected model). All the predictor variables were *z*-transformed to increase comparability. Rates of canopy opening (negative values of canopy change) are associated with greater absolute rates of centroid shifts. The west–east rate was exclusively linked to nitrogen deposition, with faster westward shifts in species with lower rates of nitrogen deposition across their distributions. Model fit is presented as the proportion of variation explained by the fixed effect (marginal R^2, R^2_m) and the proportion of variation explained by the fixed and random effects (conditional R^2, R^2_c). Models accounted for plant growth form as random intercept (five levels: forbs, graminoids, pteridophytes, shrubs, and trees). (**B**) Results of the variation partitioning analyses representing the individual contribution of each environmental predictor. Bar plots are proportional to the variation explained by the contribution of each fixed effect (expressed as R^2_m). In all graphs, estimates and error bars represent the median value and 2.5 to 97.5 percentiles across 1000 bootstrap samples. See fig. S7 for results on the analyses that also included rare species and fig. S8 for a direct comparison with the estimated effects of acidifying deposition.

the same time. For example, we simultaneously considered changes in maximum growing-season temperatures, minimum winter temperatures, and growing-season precipitation as one measure of the climate-change velocity between the baseline survey and resurvey periods (fig. S2). This is highly relevant because plants respond not only to warming temperatures, but also to alterations in precipitation regimes. In this method, for all resurveyed vegetation plots, a grid search (at 4 km by 4 km resolution) was performed to map all raster cells within the study area in which the climatic conditions in the resurvey period are similar (i.e., show no statistical difference) to a given plot's climate during the baseline period (i.e., "analog climate conditions"). For each plot, we then located the position of the nearest raster cell with analog climatic conditions to calculate the velocity and geographic direction of climate change over time. Identical to the centroid shifts, the climate-change velocity for each plot was expressed as the absolute shift velocity (km year^{-1}), as well as the projected south–north (km north year^{-1}) and west–east (km east year^{-1}) velocity. The directionality of climate analog shifts was tested by using Rayleigh's *r* coefficient as described above.

Centroid shifts across the 266 understory plant species varied from 0.006 km year^{-1} (*Symphytum cordatum*) to 18.27 km year^{-1} (*Abies alba* seedlings) and occurred at a mean rate of 3.56 (5% to 95% quantile: 0.39 to 9.80) km year^{-1} (Fig. 2A and data S1). Unexpectedly, two-thirds of the studied plant species showed directional shifts along the west–east axis (Rayleigh's r = 0.23; df = 265; $P < 0.05$). Most of these shifts were westward (39% of species), but we also noted many eastward shifts (23%). Southward shifts (23%) were more frequent than northward shifts (15%). Westward range centroid shifts were thus 2.6 times more likely than the northward range shifts expected in response to climate change. The average south–north rate of centroid shifts was slow but significantly equatorward [−0.63 (−4.30 to 2.89) km north year^{-1}; one-sample *t* test: t = −4.36, df = 265, $P <$ 0.001], whereas the rate of west–east shifts was 1.8 times faster and significantly westward (−1.17 [−6.95 to 4.17] km east year^{-1}; one-sample *t* test: t = −4.90, df = 265, $P < 0.001$). The observed rates of centroid shifts toward each cardinal direction ranged from 62% (southward) to 70% (eastward) faster than expected by chance alone, as confirmed by a null-model approach (fig. S5).

The climate significantly changed over the course of the study period in 2949 of the 2954 resurveyed vegetation plots (99.8%) based on climate analog mapping. Maximum growing-season temperatures increased by an average of 1.59 (1.15 to 2.21) °C. Climate change took place at an average absolute velocity of 0.66 (0.07 to 1.67) km year^{-1} (Fig. 2B). Unsurprisingly, the dominant geographic direction of climate change was north (40% of the plots; Rayleigh's r = 0.29; df = 2,948; $P < 0.05$). The south–north velocity of climate change was also significantly northward [0.24 (−0.72 to 1.94) km north year^{-1}; one-sample *t* test: t = 18.15, df = 2,948, $P < 0.001$]. The west–east climate-change velocity was marginal but significantly eastward [0.06 (−0.92 to 0.72) km east year^{-1}; one-sample *t* test: t = 5.55, df = 2,948, $P < 0.001$] and thus

Downloaded from https://www.science.org at Universitaetsbibliothek Bern on October 15, 2024

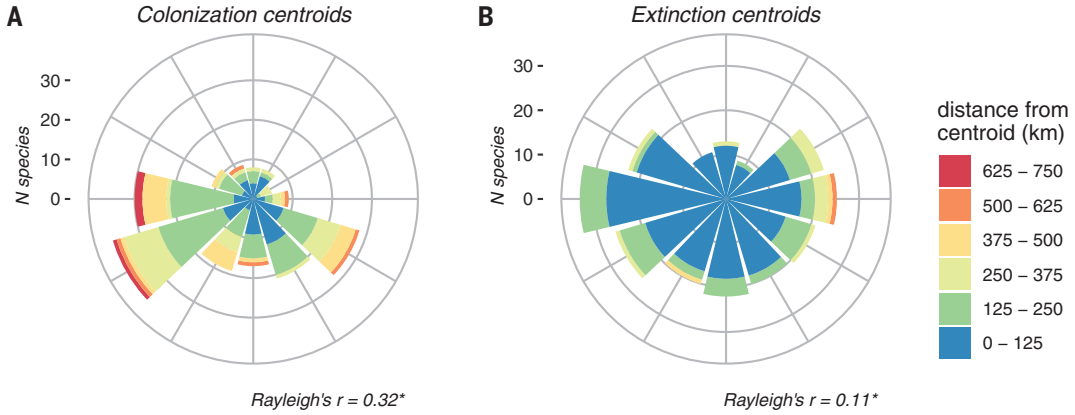

Fig. 4. Distance and geographic direction of colonization and extinction centroids. (**A**) Distance and geographic direction of colonization centroids (*n* species = 202). (**B**) Distance and geographic direction of extinction centroids (*n* = 246). Longer distances reflect that colonization or local extinction are happening in one preferred direction relative to the baseline centroid. Rayleigh's *r* statistic represents a test of uniformity that compares the bearings of shifts to a uniform circular distribution (null hypothesis). Larger values indicate more directed shifts. Asterisk (*) indicates significant deviations from the null hypothesis ($P < 0.05$). Results of the analyses that also included rare species are presented in fig. S9. Results for each biogeographic region are presented in fig. S10.

opposite to the most common cardinal direction of centroid shifts of European forest plants.

Neither the geographic direction nor the velocity of climate change was reflected in the species' centroid shifts, which hints toward the importance of other environmental changes. Two prominent alternative drivers of forest plant community changes are elevated atmospheric inputs of nitrogen and forest canopy cover changes (*16*, *25*–*28*), with eutrophying effects of nitrogen complicated by recovery dynamics from past acidification caused by the combined deposition of nitrogen and sulfur compounds (*29*, *30*). These drivers show spatial patterns not confounded with the velocity of climate change (across all plots, pairwise Spearman correlations between the south–north velocity of climate change versus the rates of nitrogen deposition and forest canopy cover changes were only 0.04 and 0.01, respectively).

To better understand the potential drivers associated with the reported changes in the geographical distribution of species, we related the rates of centroid shifts to the average rate of nitrogen deposition between the baseline survey and resurvey (kg N ha^{-1} $year^{-1}$) extracted from atmospheric deposition maps at 0.1° resolution (~8 km by 8 km within the study area) (Fig. 1A) and to the observed rate of forest canopy cover change at each site (percent canopy cover increase $year^{-1}$) while also accounting for the velocity of climate change (the absolute, south–north, and west–east velocity) in a linear mixed-effects modeling framework. We furthermore tested for the potential confounding effect of past acidifying deposition, considering the known adverse effects on European forest plant communities (*31*). The acidifying deposition rate, however, was highly correlated to the rate of nitrogen deposition over the course of the study because of partially shared emission sources (Spearman correlation: 0.87; *n* = 2954 plots), and their individual effects are therefore difficult to tease apart in an observational study. We calculated species-specific experienced rates of atmospheric (nitrogen and acidifying) deposition and forest canopy cover changes as the average rate across all plots where the species was observed, weighted by the species' original abundance in the baseline time period survey (fig. S6 for a data flow chart).

Model outputs show that the absolute rate of centroid shifts was weakly but exclusively linked to the rate of forest canopy change, with greater opening of the canopy enhancing centroid shifts (Fig. 3). The velocity of climate change was not associated with the rates of centroid shifts. By contrast, the rate of nitrogen deposition was significantly linked to the west–east rate of centroid shifts, with species that initially experienced a lower nitrogen deposition rate across their distributions showing faster westward shifts (Fig. 3A). Variation partitioning revealed that the nitrogen deposition rate, rather than the climate-change velocity, explained most of the variation in the species' centroid shifts, albeit the proportion of variation explained was small (Fig. 3B and fig. S7). The estimated effects of past acidifying deposition on species centroid shifts were nearly identical to the effects of the spatially correlated nitrogen deposition rate (fig. S8). We are therefore unable to distinguish with certainty whether centroid shifts were brought about by eutrophying rather than changes in acidifying deposition or a combination of both. In either case, however, atmospheric deposition rates—and not the climate-change velocities—were the superior predictors of westward species movements.

Colonization and extinction centroids

To shed light on the mechanisms that drive centroid shifts, we decomposed centroid shifts into shifts attributed to the individual contribution of colonization and local extinction. For this analysis, we introduce the concept of colonization centroids (the centroid of plots newly colonized by a species, abundance weighted by the percentage cover in the resurvey) and extinction centroids (the centroid of plots in which a species became extinct, abundance weighted by the percentage cover in the baseline survey). Colonization and extinction centroids were expressed as the projected distance from the species' baseline centroid position in each geographic direction (kilometers north and kilometers east). From a biogeographical point of view, longer distances reflect that colonization or local extinction events took place farther away from the baseline and that these processes occurred mostly in one preferred direction (schematically explained in fig. S1C).

The average absolute distance of colonization centroids [202.20 (28.30 to 478.46) km; *n* species = 202] was larger than the average absolute distance of extinction centroids [82.22 (4.22 to 249.48) km; *n* species = 246; Fig. 4 and figs. S9 and S10]. Colonization centroids were also more isotropic across species (Rayleigh's $r = 0.32$; df = 201; $P < 0.05$) than extinction centroids (Rayleigh's $r = 0.11$; df = 245; $P < 0.05$). This suggests that colonization events were happening more in one preferred direction and occurred further away from baseline centroids (i.e., closer to range boundaries) compared with local extinctions.

Colonization along the west–east axis was most closely related to the nitrogen deposition rate (figs. S11 and S12). Because the observed dominant direction of species' colonization was westward (39% of the species colonized west, 21% east, 28% south, and 12% north), colonization occurred more frequently for species that initially experienced a lower rate of nitrogen depositions across their distributions. This pattern is possibly associated with the westward colonization of nitrogen generalist species that can take advantage of eutrophic conditions such as observed in large parts of Western Europe (Fig. 1A and fig. S13). Indeed, linking the colonization centroids to each species' ecological indicator value for nitrogen niche width (with larger values indicating generalist species with a broader niche) (*32*) revealed that, for nitrogen generalists in

Downloaded from https://www.science.org at Universitaetsbibliothek Bern on October 15, 2024

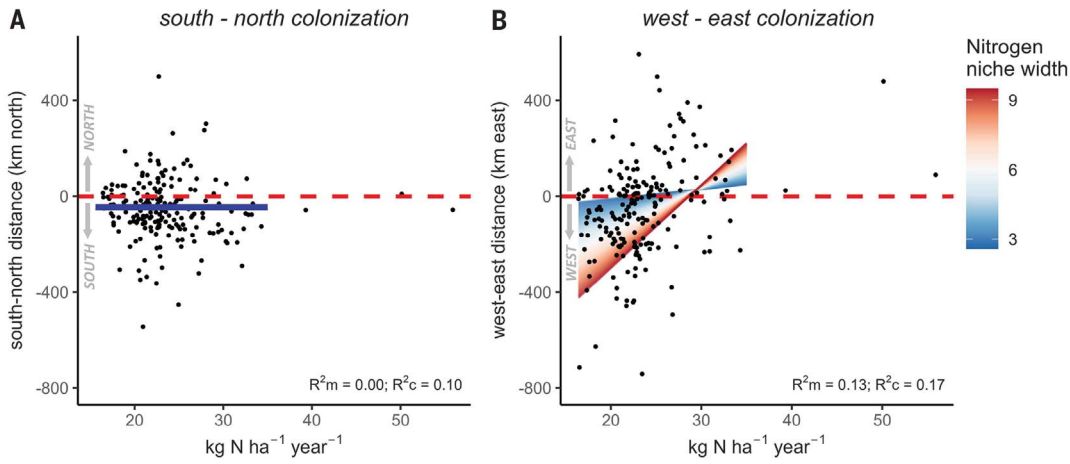

Fig. 5. Effects of nitrogen deposition rates and species nitrogen niche width on colonization centroids. (**A** and **B**) Results of the mixed-effects model testing for the interaction effect between the average nitrogen deposition rate between the baseline survey and resurvey across each species' distribution (kg N ha^{-1} $year^{-1}$) and species' ecological indicator values for nitrogen niche width (an index integrating the intra- and inter-regional variability in the nitrogen niche, with higher values indicating more generalist species and smaller values specialist species) on the south–north and west–east colonization centroids. Negative distances indicate southward (A) or westward colonization (B). Interaction effects between species nitrogen niche width and the average nitrogen deposition rate between the baseline survey and resurvey across each species' distribution are plotted along the color gradient. Model predictions were plotted to a maximum of 35 kg N ha^{-1} $year^{-1}$ to avoid extrapolation uncertainty for deposition values where observations were scarce. Modeling results without outlier data (n = 3 data points) are provided in fig. S13. The most parsimonious model of south–north colonization was an intercept-only model (blue solid line). Westward colonization depended on species nitrogen niche width. Nitrogen generalists that initially occurred in areas with lower rates of nitrogen deposition moved more westward. Colonization in the more specialist species was generally suppressed, irrespective of the nitrogen deposition rate. In all plots, the red dashed line represents the zero line.

particular, those that initially occurred in areas with a lower rate of nitrogen deposition have taken advantage to move more westward (Fig. 5 and fig. S14). Nitrogen generalists that already occurred in areas with higher nitrogen deposition (Western Europe; Fig. 1A and fig. S13) tended to remain in place without necessarily moving westward. More specialist species—i.e., those with narrow niche widths for nitrogen and that often also have smaller range sizes (*33*)—have shown lower colonization rates across temperate Europe, allowing generalist species to replace specialists (*14*). Also, the decreasing levels of acidifying deposition [since the peak in the 1980s (*34*)] may have facilitated the recovery of species' ranges in formerly polluted regions (*30*). Using our observational data, we cannot fully disentangle these recovery effects after past acidification caused by both nitrogen and sulfur pollution from dynamics of eutrophication chiefly involving nitrogen deposition. However, eutrophication may be the most likely driver because (i) we show that west–east colonization distances were statistically better linked to nitrogen deposition and the species' nitrogen niche width than to acidifying deposition and the species acidity niche width (fig. S15) and (ii) most of the vegetation plots appear to be relatively well-buffered against soil acidification (fig. S16). Regardless of whether the driver of westward colonization chiefly involves eutrophying deposition or facilitated by the recovery from past acidification, forest plant species native to regions with lower atmospheric deposition rates are more vulnerable to unanticipated range shifts in response to atmospheric pollution—a key finding for forest biodiversity conservation policy.

Local extinction events along the south–north axis were preferentially located southward relative to the species' baseline centroid position and thus closer to species' warm range limits (25% south versus 13% north) (Fig. 4). This trend was significantly associated with climate change and a higher rate of nitrogen deposition (figs. S11 and S12). Local extinction events along the west–east axis, however, occurred more often (28% east and 31% west). Eastward local extinctions occurred more commonly in species that experienced a higher rate of nitrogen deposition across their distribution. Such nitrogen-mediated local extinctions were amplified when forest canopies became more open. The velocities of climate change also interacted with the rate of forest canopy cover change in that local extinctions due to climate change occurred more often in forests where the canopy cover decreased. This confirms the importance of tree canopies in buffering the impacts of environmental changes (*35*).

Our findings suggest that atmospheric deposition and forest canopy cover dynamics interact to determine how forest plant species are shifting their ranges and that these environmental changes induce shifts that can be independent from isotherm shifts. This contradicts the idea that species have shifted ranges mainly in response to warming air temperatures. Rather, other environmental changes, especially rates of atmospheric deposition and forest canopy cover dynamics, have likely induced unexpected westward range shifts in European forest plants. Although it remains unclear whether the effect of atmospheric deposition chiefly involves eutrophication or a recovery effect from past acidification due to both nitrogen and sulfur pollution, our findings point at nitrogen deposition as the most likely driver explaining the westward range shifts in European forest plants. Since the continued success of the United Nations air convention and the European Union Emissions Ceiling Directive in reducing nitrogen and sulfur emission levels, prospective trends in climate change and atmospheric deposition are unlikely parallel, with climate change outpacing the effects of atmospheric deposition on future species' range shifts. Accurate and recent range shift data will be key to adequately anticipating the respective impacts of climate change and atmospheric deposition on biodiversity and ecosystem functioning. It is already clear, however, that biodiversity redistribution patterns appear complex and are more likely driven by the interplay among several environmental changes than due to the exclusive effect of climate change alone.

REFERENCES AND NOTES

1. J. Lenoir *et al.*, *Nat. Ecol. Evol.* **4**, 1044–1059 (2020).
2. I.-C. Chen, J. K. Hill, R. Ohlemüller, D. B. Roy, C. D. Thomas, *Science* **333**, 1024–1026 (2011).
3. M. T. Burrows *et al.*, *Science* **334**, 652–655 (2011).
4. J. W. Williams, S. T. Jackson, *Front. Ecol. Environ.* **5**, 475–482 (2007).
5. C. Parmesan *et al.*, *Nature* **399**, 579–583 (1999).
6. J. Lenoir, J. C. Gégout, P. A. Marquet, P. de Ruffray, H. Brisse, *Science* **320**, 1768–1771 (2008).
7. R. Virkkala, A. Lehikoinen, *Glob. Change Biol.* **20**, 2995–3003 (2014).
8. S. Dullinger *et al.*, *Nat. Clim. Chang.* **2**, 619–622 (2012).
9. C. Parmesan, G. Yohe, *Nature* **421**, 37–42 (2003).

Downloaded from https://www.science.org at Universitaetsbibliothek Bern on October 15, 2024

10. M. A. Rubenstein *et al*., *Environ. Evid.* **12**, 7 (2023).
11. L. P. Shoo, S. E. Williams, J. Hero, *Austral Ecol.* **31**, 22–29 (2006).
12. J. D. Ash, T. J. Givnish, D. M. Waller, *Glob. Change Biol.* **23**, 1305–1315 (2017).
13. T. L. Greaver *et al*., *Nat. Clim. Chang.* **6**, 836–843 (2016).
14. I. R. Staude *et al*., *Nat. Ecol. Evol.* **4**, 802–808 (2020).
15. C. Senf, R. Seidl, *Nat. Sustain.* **4**, 63–70 (2021).
16. P. Sanczuk *et al*., *Nat. Clim. Chang.* **13**, 840–847 (2023).
17. S. M. Crimmins, S. Z. Dobrowski, J. A. Greenberg, J. T. Abatzoglou, A. R. Mynsberge, *Science* **331**, 324–327 (2011).
18. D. Jacobsen, *Front. Ecol. Environ.* **18**, 211–218 (2020).
19. J. Lenoir *et al*., *Ecography* **33**, 295–303 (2010).
20. D. M. Olson *et al*., *Bioscience* **51**, 933–938 (2001).
21. J. Vanderwal *et al*., *Nat. Clim. Chang.* **2**, 1–5 (2012).
22. M. C. Fitzpatrick, R. R. Dunn, *Nat. Commun.* **10**, 614 (2019).
23. J. W. Williams, S. T. Jackson, J. E. Kutzbach, *Proc. Natl. Acad. Sci. U.S.A.* **104**, 5738–5742 (2007).
24. S. R. Loarie *et al*., *Nature* **462**, 1052–1055 (2009).
25. P. De Frenne *et al*., *J. Ecol.* **101**, 784–795 (2013).
26. J. Segar *et al*., F. *Nat. Commun.* **13**, 7837 (2022).
27. K. Verheyen *et al*., *J. Ecol.* **100**, 352–365 (2012).
28. P.-O. Hedwall *et al*., *Glob. Ecol. Biogeogr.* **30**, 1765–1780 (2021).
29. N. Duarte, L. H. Pardo, M. J. Robin-Abbott, *Water Air Soil Pollut.* **224**, 1355 (2013).
30. E. Tipping, J. A. C. Davies, P. A. Henrys, S. G. Jarvis, S. M. Smart, *Environ. Pollut.* **281**, 117017 (2021).
31. G. Riofrío-Dillon, R. Bertrand, J.-C. Gégout, *Glob. Change Biol.* **18**, 3383–3394 (2012).
32. J. Dengler *et al*., *Veg. Classif. Surv.* **4**, 7–29 (2023).
33. S. Kambach *et al*., *Ecography* **42**, 467–477 (2019).
34. P. Grennfelt *et al*., *Ambio* **49**, 849–864 (2020).
35. P. De Frenne, *Nat. Ecol. Evol.* **8**, 196–202 (2024).
36. J. T. Abatzoglou, S. Z. Dobrowski, S. A. Parks, K. C. Hegewisch, *Sci. Data* **5**, 170191 (2018).
37. EMEP, Transboundary particulate matter, photo-oxidants, acidifying and eutrophying components (EMEP Status Report 1/2023, Norwegian Meteorological Institute, 2023); https://emep.int/publ/reports/2023/EMEP_Status_Report_1_2023.pdf.
38. European Environment Agency, https://www.eea.europa.eu/en/datahub/datahubitem-view/.
39. P. Sanczuk *et al*., Data and Code associated with original research article: Unexpected westward range shifts in European forest plants link to nitrogen deposition [Dataset], Dryad; https://doi.org/10.5061/dryad.4b8gthtmt (2024).

ACKNOWLEDGMENTS

This paper is an outcome of the sREplot working group supported by sDiv, the Synthesis Centre of the German Centre for Integrative Biodiversity Research (iDiv) Halle-Jena-Leipzig (DFG FZT 118). **Funding:** P.S., P.D.F., and P.V. received funding from the European Research Council (ERC) under the European Union's Horizon 2020 research and innovation program (ERC Starting Grant FORMICA 757833) and Ghent University grant BOF23/GOA/019. F.Z. received funding from the Swiss National Science Foundation (project 193645). J.J.L. received funding from the Research Foundation-Flanders (FWO, OZ7828, OZ7916 and OZ7792). K.D.P. received funding from the Research Foundation-Flanders (FWO, ASP035-19 De Pauw). I.B. was supported by means of grant EFOP-3.6.1.-16-2016-00018. A.D.B. received funding from the Knut and Alice Wallenberg Foundation (WAF KAW 2019.0202) and the Swedish Foundation for Strategic Research (FFL21-0194). M.C. was supported by the postdoctoral fellowship L200052302 of the Czech Academy of Sciences, grant 21-11487S by the Czech Science Foundation. M.K., R.H., M.C., O.V., M.M., and P.P. were supported by the Czech Academy of Sciences (RVO 67985939). T.Di. received funding from the eLTER PLUS project of the European Union Horizon 2020 (INFRAIA-01-2018-2019). C.G. received funding from FORMAS (project 2021-01993). R.H. was supported by the Czech Science Foundation project 21-11487S. F.M. was supported by the project APVV-19-0319. F.R.-S. was supported by VI PPIT – US. **Author contributions:** P.S. and P.D.F. conceived the ideas and designed the methodology, with contributions of J.L., J.L.L., and F.R.-S.; all authors collected data; P.S. analyzed data in collaboration with P.D.F.; P.S. led the writing of the manuscript in collaboration with P.D.F. and with notable contributions of K.V., J.L., F.Z., J.J.L., F.R.-S., L.B., M.B.-R., K.D.P., P.V., and M.P.P.; all authors contributed critically to the draft and gave final approval for publication. **Competing interests:** The authors declare that they have no competing interests. **Data and materials availability:** Raw macroclimate data can be accessed through the TerraClimate database (*36*). Historical nitrogen and sulfur deposition data can be accessed through the EMEP/CEIP 2023 Present state of emission data-base (*37*). Shapefile of biogeographical regions are provided by the European Environment Agency (*38*). Species' ecological indicator values of nitrogen niche width are provided by Dengler *et al*. (2023) (*32*). Raw data on species centroid shifts, environmental change data, and R scripts to reproduce the methods, analyses and source code of all figures are available on Dryad (*39*). **License information:** Copyright © 2024 the authors, some rights reserved; exclusive licensee American Association for the Advancement of Science. No claim to original US government works. https://www.sciencemag.org/about/science-licenses-journal-article-reuse

SUPPLEMENTARY MATERIALS

science.org/doi/10.1126/science.ado0878
Materials and Methods
Figs. S1 to S16
References (*40*–*59*)
MDAR Reproducibility Checklist
Data S1

Submitted 22 January 2024; accepted 5 September 2024
10.1126/science.ado0878

Downloaded from https://www.science.org at Universitaetsbibliothek Bern on October 15, 2024